Tunneling and the kinetic isotope effect in $CH_3 + CH_4 \rightarrow CH_4 + CH_3$: An application of semiclassical transition state theory

Timothy A. H. Burd, Xiao Shan, David C. Clary

Physical and Theoretical Chemical Laboratory, South Parks Road, Oxford, OX1 3QZ, United Kingdom

Abstract

One-dimensional semiclassical transition state theory is applied to study the rate constants of the $CH_3 + CH_4$ reaction and its hydrogen-substituted isotopic analogues. This requires calculation of vibrational frequencies at the reactant, product and transition states, and the anharmonic constants of the reaction coordinate at the transition state. The reactions studied have a hindered rotor vibration at the transition states, whose behaviour is approximated using two methods. The results show very good agreement to experimental and other theoretical results. The three reactions studied allow evaluation of both primary and secondary kinetic isotope effects in the title reaction.

Keywords: Semiclassical transition state theory, Kinetic isotope effect, Hindered rotor, Hydrogen exchange

1. Introduction

Calculating the rate constants of chemical reactions is a key component of modern theoretical chemistry. Whilst sophisticated quantum reactive scattering (QRS) calculations are able to provide accurate results, they are typically limited to small systems (up to 7 atoms[1, 2]) due to the complexity in both constructing a full-dimensional potential energy surface (FD PES) and solving the nuclear Schrödinger equation[3]. Ring Polymer Molecular Dynamics (RPMD) has simplified the process of solving the Schrödinger equation, and is exact in the high temperature and the parabolic barrier limits, however a FD PES is still required[4–6]. Other techniques such as variational transition state theory (VTST) do not require a full PES[7]. These are based on classical transition state theory (TST), but minimise the effect of the no-recrossing assumption by optimising the position of the transition state such as to minimise the flux through the dividing surface[7]. Tunneling corrections can be incorporated via a transmission coefficient calculated using multidimensional imaginary-action integrals[8].

Semi-classical transition state theory (SCTST), developed by Miller *et al.* [9–11] requires only two molecular geometries to be identified and analysed: the 'reactant' state, and the 'transition' state (TS). SCTST is also exact in the parabolic barrier limit. Using vibrational perturbation theory, the semi-classical tunneling probability can

☆Fully documented templates are available in the elsarticle package on CTAN.
Email addresses: timothy.burd@chem.ox.ac.uk (Timothy A. H. Burd), xiao.shan@chem.ox.ac.uk (Xiao Shan), david.clary@chem.ox.ac.uk (David C. Clary)

be derived, from which the reaction rate constant can be computed. Wagner[12] suggested further modifications in order to obtain the correct behaviour in the deep tunnelling regime.

However, FD SCTST scales poorly with the system size due to both the calculation of anharmonic constants and the number of possible vibrational states. While the Wang-Landau algorithm [13] and its implementation for parallel architectures [14] have been employed to tackle the latter of these two scaling problems, the anharmonic constant calculation (which requires up to fourth order derivatives of the PES) remains a significant computational expense[15].

An alternative approach is to use SCTST within a reduced dimensionality (RD) framework, as developed and tested recently by Greene *et al.* [15–17] and Shan *et al.*[18]. In this method, only a subset of the internal degrees of freedom (DoFs) are treated anharmonically, while the remaining 'spectator' vibrational modes are treated using a simple harmonic oscillator model[17]. In doing so, this approximate method is able to tackle both scaling problems in FD SCTST. Since the anharmonic constant calculation is limited to only a small number of vibrational modes, third and fourth order derivatives of the PES only with respect to these modes are required from *ab initio* calculations. In addition, the full set of vibrational states for 1 or 2 DoFs can be enumerated with very little computational cost[13, 15].

In this work, 1D-SCTST is applied to isotopic variants of the title reaction:

$$CH_3 + CH_4 \longrightarrow CH_4 + CH_3 \qquad \text{(R1)}$$

$$CH_3 + CDH_3 \longrightarrow CDH_3 + CH_3 \qquad \text{(R2)}$$

$$CD_3 + CD_4 \longrightarrow CD_4 + CD_3 \qquad \text{(R3)}$$

Reaction R1 is known to be significant in combustion and decomposition processes[19], and so accurate rate constant values are of importance. This reaction is also used as a model for other reactions in its reaction class of a light atom transferring between two heavy molecules[20]. As such, it has been studied extensively both experimentally[21–23] and theoretically[24–30]. As it involves the transfer of a light atom, tunnelling is expected to be significant. Comparison of R1 to R2 will exhibit primary kinetic isotope effects, whilst comparison of R2 and R3 will show secondary isotope effects. These results can be compared to those calculated through reduced dimensional quantum reactive scattering calculations performed by Remmert *et al.*[24].

An interesting feature of these reactions is that a hindered-rotor vibrational mode is present in the TS. At low temperatures, these behave like molecular vibrations, whilst in the high temperature limit they behave like free rotors. Ellingson *et al.*[31] have described several practical approximation schemes for calculating the partition function of torsional modes; these range from full-dimensional path integral methods to one-dimensional approximations with analytical formulae. Since the HR vibrational mode is only found in the TS and not in

either of the reactants, this reaction provides an opportunity to study the effect of different treatments to the HR partition function. In this work, we use two methods of treatment of the HR; an analytic approximation suggested by Truhlar *et al.*[32] to move smoothly between the harmonic and free rotor behaviours, and eigenvalue summation of the 1D rotor. These are compared to a simple harmonic approximation.

The remainder of this letter is organised as follows. In Section 2 we provide a theoretical overview of SCTST and treatments of the hindered rotor degree of freedom. In Section 3, we describe the computational methods used to carry out the calculations. In Section 4 the results of the calculations and the calculated kinetic isotope effects are discussed. The key conclusions of this work are then discussed in Section 5.

2. Theory

2.1. Semi-classical Transition State Theory (SCTST)

A full description of the SCTST method in full and reduced dimensions is presented by Greene *et al.*[33]. Here, a very brief overview is provided. SCTST calculates reaction probabilities directly from harmonic frequencies, ω_i, and anharmonic constants, x_{ij}, of the reactant and transition states. In its original formulation[9], second order vibrational perturbation theory (VPT2)[34] was used to calculate anharmonic constants (VPT2 can be extended to VPT4[35] although this requires considerable extra computational effort). This requires up to fourth order derivatives of the potential along all degrees of freedom, and is thus computationally expensive for large systems. In 1D-SCTST, it is assumed the reaction mode is not coupled with the rest of the vibrational (spectator) modes in the TS. In such calculations, only the reaction mode is anharmonic, and its anharmonic constant, x_{FF}, can be calculated from the curvature of the PES at the TS,

$$x_{FF} = \frac{\hbar^2}{16\omega_F^2}\left(f_{FFFF} - \frac{5f_{FFF}^2}{3\omega_F^2}\right) \tag{1}$$

where f_{FFF} and f_{FFFF} are the third and fourth order derivatives of the potential with respect to the reaction mode coordinate. These derivatives can be estimated using numerical differentiation. Richardson Extrapolation can be used to improve the results[33], whereby *ab initio* single point energies are calculated at small displacements along the reaction coordinate either side of the transition state.

Within the VPT2 treatment, a constant energy parameter, G_0, should be added to the harmonic adiabatic reaction energy barrier. Its 1D form is given by

$$G_0 = \frac{\hbar^2}{64}\left(\frac{f_{FFFF}}{\omega_F^2} - \frac{5}{9}\frac{f_{FFF}^2}{\omega_F^4}\right). \tag{2}$$

A barrier penetration integral, $\theta(E)$, can be calculated using WKB theory,

$$\theta(E) = \pi\frac{-\omega_F + \left[\omega_F^2 + 4x_{FF}\left(\Delta V_f + G_0 - E\right)\right]^{1/2}}{2x_{FF}}. \tag{3}$$

The canonical rate constant, $k(T)$, can then be found from a Boltzmann average of the semi-classical tunnelling probability[36], given by

$$k(T) = \frac{Q^{\ddagger}}{2\pi\hbar Q_r} \int_{E_0}^{\infty} \mathrm{d}E \; e^{-\beta E} P_{SC}(E) \tag{4}$$

where

$$P_{SC}(E) = \frac{1}{1 + e^{2\theta(E)}} \tag{5}$$

and Q_r is the partition function (per unit volume) of the reactant species and E_0 is the quantum mechanical reaction threshold. $Q^{\ddagger}$ includes the electronic, rotational and translational partition functions of the TS as well as the vibrational partition function of the spectator modes.

Wagner[12] pointed out this procedure gives qualitatively incorrect results for tunnelling at low energies. The VPT2 procedure reproduces the behaviour of the barrier near the transition state, but does not incorporate the forward or reverse barrier height, thus giving the incorrect asymptotic tunnelling behaviour. This can be avoided by modeling the potential as a piecewise continuous asymmetric Eckart potential that consists of three parts. This potential function maintains the analyticity of $\theta(E)$ whilst giving the correct asymptotic behaviour. This method also requires calculation of the reverse barrier height, thus the products region must be identified and analysed as well. Within the one-dimensional framework, all products and reactant normal modes can be treated purely harmonically, as the reaction mode is not present in these states. Note that since all three reactions are symmetric, no additional computation is required to determine the properties of the product states.

To show the contribution of quantum tunneling to the reaction, we compare the 1D-SCTST results to the standard TST rate constants, given by

$$k(T) = \frac{Q^{\ddagger}}{2\pi\hbar Q_r} \left(kT \; e^{-E^{\ddagger}/kT} \right). \tag{6}$$

Note that in 1D-SCTST, $Q^{\ddagger}$ is the same as that of a standard TST calculation.

2.2. Treatment of the hindered rotor

Hindered rotational modes present a challenge to treat in a simplified manner. Whilst expensive treatments include the effects of torsional mode coupling and the existence of multiple, distinguishable conformers[37], here we focus on simplified treatments. An initial assumption is that the hindered rotor is separable from all other vibrational degrees of freedom. This is justified by noting that the frequency of a hindered rotor vibration is typically at least an order of magnitude less than other vibrations. Moreover, it can be verified that when projecting the hindered rotor degree of freedom out of the Hessian matrix, the post-projection vibrational frequencies change very little. The separability of some vibrational degrees of freedom is also implicit in reduced-dimensionality approaches to SCTST. Thus the partition function can be written as the product of

a vibrational part and a rotor part, and the problem is reduced to one-dimension. Hindered rotations can be approximated as harmonic oscillators in the low temperature limit, or free rotors in the high temperature limit, and various approximate treatments have been suggested for the whole temperature range. Several methods (ranging from very approximate, to more detailed) have been suggested, as reviewed by Lin *et al.*[38]. Here, we discuss two methods. In order to investigate the effects of these treatments, we compare these results to that of a calculation using a normal harmonic oscillator partition function.

Truhlar and coworkers[32] have suggested an approximation for the rotor; a function that moves smoothly from the harmonic oscillator partition function to the free rotor partition function as T increases,

$$Q = Q^{\mathrm{HO}} \tanh(Q^{\mathrm{FR}}/Q^{\mathrm{I}}) \tag{7}$$

where

$$Q^{\mathrm{HO}} = \frac{e^{-\hbar\omega/2kT}}{1 - e^{\hbar\omega/kT}} \tag{8}$$

is the partition function for the low temperature harmonic oscillator approximation,

$$Q^{\mathrm{FR}} = \frac{(2\pi I_m kT)^{1/2}}{\hbar\sigma} \tag{9}$$

is the partition function for a free rotor, and

$$Q^{\mathrm{I}} = \frac{kT}{\hbar\omega} \tag{10}$$

is the high temperature limit of the harmonic oscillator partition function. The reduced moment of inertia, I_m, can be calculated in curvilinear coordinates from an expression that is exact for symmetric tops[39],

$$I_m = A_m \left(1 - \sum_{i=1}^{3} A_m \lambda_{mi}^2 \; I_i \right) \tag{11}$$

where A_m is the moment of inertia for the rotating top, λ_{mi} is the direction cosine between the m^{th} top and the i^{th} principal axis of the molecule, and I_i is the moment of inertia of the whole molecule about this axis. This quantity can also be calculated in rectilinear coordinates:

$$I_m = \frac{I_1 I_2}{I_1 + I_2} \tag{12}$$

where I_1 and I_2 are the moments of inertia of the two tops rotating relative to one another about the axis of rotation. These two are equivalent in the case that $I_1 + I_2 = I_i$, which is the case for the reactions investigated here. Equation (7) will be referred to, in the following, as the 'tanh' approximation for the hindered rotor.

The partition function can also be found numerically by solving the rotational Schrödinger equation for the system with the Hamiltonian:

$$\mathcal{H} = \frac{\partial}{\partial\theta} B(\theta) \frac{\partial}{\partial\theta} + V(\theta) \tag{13}$$

where θ is the angle of the rotation, and $B(\theta)$ is the effective rotational constant[39]. For a spherical top, $B(\theta)$ is independent of θ, simplifying the equation. The barrier height can be determined from a torsional scan, and the rotor potential can then be approximated as

$$V(\theta) = W\cos(3\theta) \tag{14}$$

where W is the barrier height. This was found to be adequate to accurately approximate the torsional potential surface. Equation (13) is then be solved to find a spectrum of eigenvalues, which determine the partition function. Calculating the partition function from the eigenvalues of equation (13) is referred to in the following as the 'numerical solution' to the hindered rotor, and is assumed to be the most accurate treatment presented here.

Whilst previous SCTST calculations have made use of the tanh method of Truhlar *et al.*[18, 33], these all contained similar hindered rotors in both the reactant and transition states; thus errors are likely to cancel. In reactions R1, R2 and R3, a hindered rotor is present only in the transition state, and so its detailed treatment is more important, and it is possible to evaluate the errors associated with each.

3. Computational Methods

3.1. ab initio Calculations

Single point energy calculations were performed at the CCSD(T)/cc-pVTZ // MP2/cc-pVTZ[40] level of theory in Gaussian 09[41]. Energy calculations using cc-pVQZcc and cc-pV5Z basis sets were also performed, allowing extrapolation to the complete basis set (CBS)[42]. For optimising the transition states, a *tight* convergence criteria was used, as suggested by Barone[34] for calculating anharmonic constants.

Vibrational frequencies were calculated at the MP2/cc-pVTZ level of theory. The anharmonic constant for the reaction coordinate was calculated by determining the energy at the MP2 level at 9 points along the reaction coordinate, in the vicinity of the transition state, and using second order Richardson extrapolation as described by Greene *et al.*[33]. Previous studies[18, 33] have suggested this order of extrapolation is sufficient to give converged derivatives for a typical barrier. A step size of $\Delta Q = 0.02$ (a.m.u.)$^{0.5}$ a_0 was used.

4. Results and discussion

4.1. Stationary point analysis

The geometry of the transition state is shown in Fig. 1 and the harmonic frequencies of each of the stationary points before and after projecting out the HR degree of freedom are shown in Table 1. Compared to the transition state of R1, the transition states of R2 and R3 have lower imaginary frequencies due to the increased mass of the central atom, corresponding to a flatter barrier curvature. The hindered rotor frequency is significantly lower in R3, where the rotating atoms have increased in mass. After projecting out the hindered rotor degree

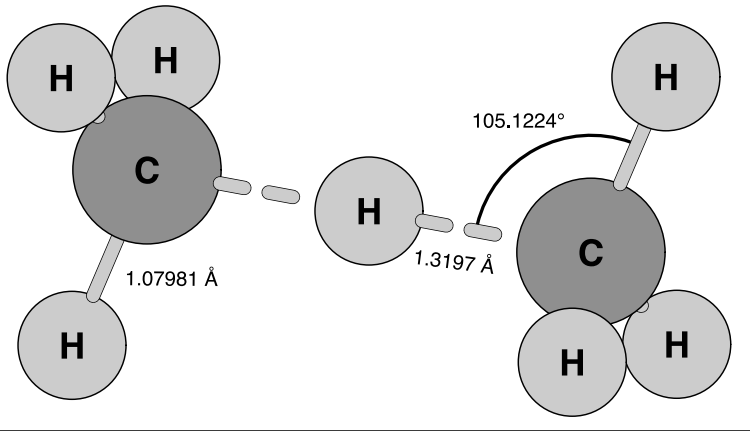

Figure 1: Transition state for reaction (R1). Within the Born-Oppenheimer approximation, the geometry is unchanged under isotopic substitution.

of freedom, the vibrational frequencies change very little indicating the separability assumption is good. The classical reaction barrier is shown in Table 2 at different levels of theory. Increasing the size of the basis set lead to a decrease in barrier height of approximately 0.6 kJ/mol. The barrier used is about 1 kJ/mol smaller than that of Ramazani *et al.* and 1 kJ/mol larger than that calculated by Temelso *et al.*[27]. Other transition state data are shown in Table 3.

4.2. SCTST results

4.2.1. $CH_3 + CH_4 \longrightarrow CH_4 + CH_3$

The most accurate treatment of the hindered rotor used in this study is numerically solving the Schrödinger equation. The results of the SCTST calculation using this method are compared to 2D-QRS calculations by Remmert *et al.*[24] and experimental results[21, 22] in Fig. 2 (a), showing good agreement. 1D-SCTST can be seen to underestimate the experimental rates and the results of 2D-QRS calculations. 1D-SCTST gives a rate about 3 times lower than the 2D-QRS result at 500 K; moreover the results do not converge exactly at high temperature, where tunneling effects are negligible.

Note that our 1D-SCTST calculation was performed at a different level of theory to the 2D-QRS results[24], however the difference in the adiabatic energy barrier height in the two calculations is less than 0.5% (75.3954 kJ/mol for 1D-SCTST and 76.0895 kJ/mol for 2D-QRS) and so should have negligible effect on the estimated rate constants. In the current study, we employ methods that compute the hindered rotor partition function more accurately than that used in the 2D-QRS calculation. As discussed in Section 2.2, a hindered rotor behaves similarly to a free rotor at higher temperature; this may be the cause of the discrepancy of the two rate constants in this range. To investigate this effect, we calculated the 1D-SCTST rate constant using a simple harmonic oscillator partition function for the hindered rotor mode and compared it to the 2D-QRS results in Fig. 2 (b). It can be seen that the two curves now have excellent agreement over the entire temperature range. This shows

Species	Frequencies / cm^{-1}			
CH_3	3371.91 (E)	3200.81 (A_1')	1450.38 (E)	501.209 (A_2')
CD_3	2512.89 (E)	2264.18 (A_1')	1067.21 (E)	388.537 (A_2')
CH_4	3215.66 (T_2)	3093.35 (A_1)	1599.85 (E)	1358.31 (T_2)
CDH_3	3215.39 (E)	3129.00 (A_1)	2327.97 (A_1)	1534.60 (E)
	1352.65 (A_1)	1200.95 (E)		
CD_4	2380.59 (T_2)	2188.17 (A_1)	1131.70 (E)	1026.90 (T_2)
Transition State (R1)	1931.04 **i** (A_{2u})	3262.54 (E_u)	3262.23 (E_g)	3126.78 (A_{1g})
	3125.33 (A_{2u})	1505.68 (E_u)	1474.12 (E_g)	1393.98 (E_u)
	1210.79 (A_{2u})	1169.87 (A_{1g})	714.81 (E_g)	543.73 (A_{1g})
	330.75 (E_u)	**56.00** (A_{1u})		
Transition State (R1) post	1931.03 **i** (A_{2u})	3262.52 (E_u)	3262.21 (E_g)	3126.76 (A_{1g})
	3125.31 (A_{2u})	1505.67 (E_u)	1474.11 (E_g)	1393.98 (E_u)
	1210.79 (A_{2u})	1169.86 (A_{1g})	714.81 (E_g)	543.72 (A_{1g})
	330.75 (E_u)			
Transition State (R2)	1442.21 **i** (A_{2u})	3262.48 (E_u)	3262.23 (E_g)	3126.78 (A_{1g})
	3124.77 (A_{2u})	1474.14 (E_u)	1474.12 (E_g)	1169.87 (E_u)
	1165.43 (A_{2u})	1114.22 (A_{1g})	714.81 (E_g)	543.73 (A_{1g})
	303.79 (E_u)	**56.00** (A_{1u})		
Transition State (R2) post	1442.20 **i** (A_{2u})	3262.46 (E_u)	3262.21 (E_g)	3126.76 (A_{1g})
	3124.75 (A_{2u})	1474.13 (E_u)	1474.11 (E_g)	1169.86 (E_u)
	1165.43 (A_{2u})	1114.22 (A_{1g})	714.81 (E_g)	543.72 (A_{1g})
	303.79 (E_u)			
Transition State (R3)	1421.78 **i** (A_{2u})	2423.48 (E_u)	2422.77 (E_g)	2227.77 (A_{1g})
	2223.69 (A_{2u})	1075.31 (E_u)	1073.46 (E_g)	1028.69 (E_u)
	931.37 (A_{2u})	906.14 (A_{1g})	535.25 (E_g)	479.65 (A_{1g})
	234.38 (E_u)	**39.61** (A_{1u})		
Transition State (R3) post	1421.77 **i** (A_{2u})	2423.46 (E_u)	2422.76 (E_g)	2227.76 (A_{1g})
	2223.68 (A_{2u})	1075.31 (E_u)	1073.45 (E_g)	1028.68 (E_u)
	931.36 (A_{2u})	906.14 (A_{1g})	535.24 (E_g)	479.65 (A_{1g})
	234.38 (E_u)			

Table 1: Harmonic frequencies at the stationary points in reactions R1-R3 pre- and post- projection of the hindered rotor degree of freedom. Hindered rotor frequencies are in bold. Symmetry labels are given in parenthesis and degenerate frequencies are not repeated.

the discrepancies found between 1D-SCTST and 2D-QRS is indeed due to the application of the hindered rotor partition function. In Fig. 2 (a), we also compare the 1D-SCTST rate constant to experimental results reported

MP2	CCSD(T)			
cc-pvtz	cc-pvtz	cc-pvqz	cc-pv5z	CBS
78.5064	76.0895	75.3901	75.3343	75.3954

Table 2: Classical barrier heights for the series of reactions R1-R3 calculated at different levels of theory with increasingly large basis sets. CBS is the complete basis set extrapolation[42]. Energies in kJ mol^{-1}.

Formula	x_{FF} (cm^{-1})	G_0 (kJ/mol)	W (kJ/mol)	$I_m/10^{-47}$ (kg m^2)
R1	-315.36	-0.943	0.305149	2.7278
R2	-565.35	-1.691	0.305149	2.7278
R3	-581.71	-1.740	0.305149	5.4513

Table 3: Transition state data for reactions R1-R3.

in Refs. [21, 22] . We can see that the 1D-SCTST results have better agreement to the experimental data than the 2D-QRS at higher temperature; however, there is a small underestimation at lower temperature. This is likely due to neglecting multi-dimensional tunneling effects, such as corner-cutting [43]. Multi-dimensional SCTST includes such effects, to some extent, in the calculation[16, 44], however such analyses are beyond the scope of the current study.

The results of using three different treatments of the hindered rotor are compared in Fig. 3. The harmonic oscillator overestimates the rotor partition function, giving a value about two times too large at 500 K, but converges to that of the numerical solution at low temperature (when the barrier to rotation is much larger than the thermal energy in this degree of freedom). The tanh approximation, gives excellent agreement over the whole temperature range, differing at most by 0.7 % from the numerical solution, and thus can provide an excellent approximation for this and similar systems.

4.2.2. Kinetic Isotope Effect

Both primary and secondary isotope effects can be seen by comparing reactions R1, R2, and R3, whose rates are compared in Fig. 4, where the hindered-rotor partition function was calculated numerically. The rate for R2 has been multiplied by four to account for the differences in symmetry numbers between the three reactions, allowing the rates to be compared directly. Differences in rate between R1 and R2 are due to the primary isotope effect (a result of altering the tunnelling atom). This is seen to significantly decrease the rate as a result of the heavier tunnelling atom. The decreased imaginary frequency at the transition state of R2 (compared to that of R1) indicates a flatter and thus wider barrier to tunnel, thus the rate is decreased. The decreased contribution of tunnelling can be seen in the smaller curvature in the Arrhenius plot.

Comparing R2 and R3 illustrates the secondary isotope effect caused by replacing the non-reactive hydrogen

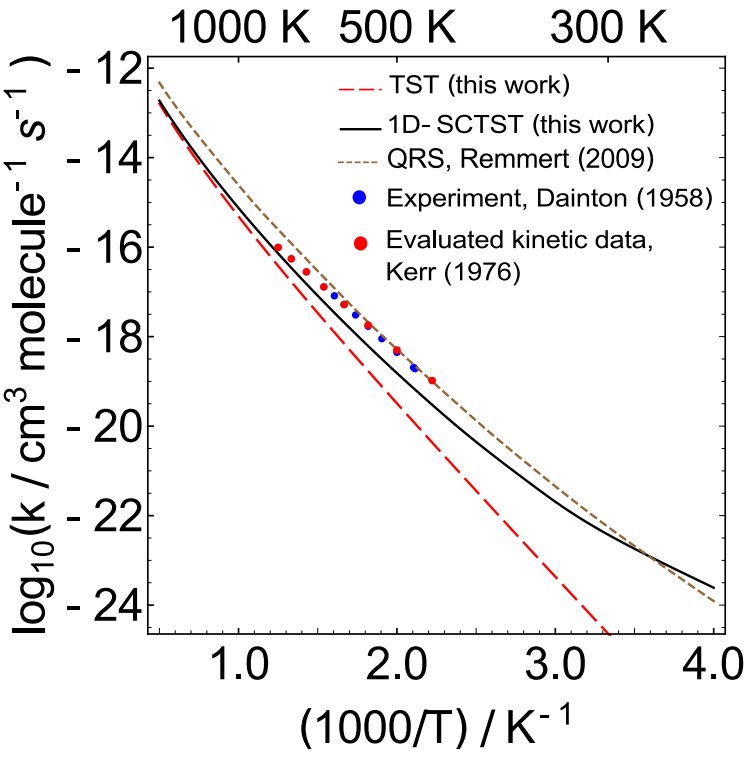

(a)

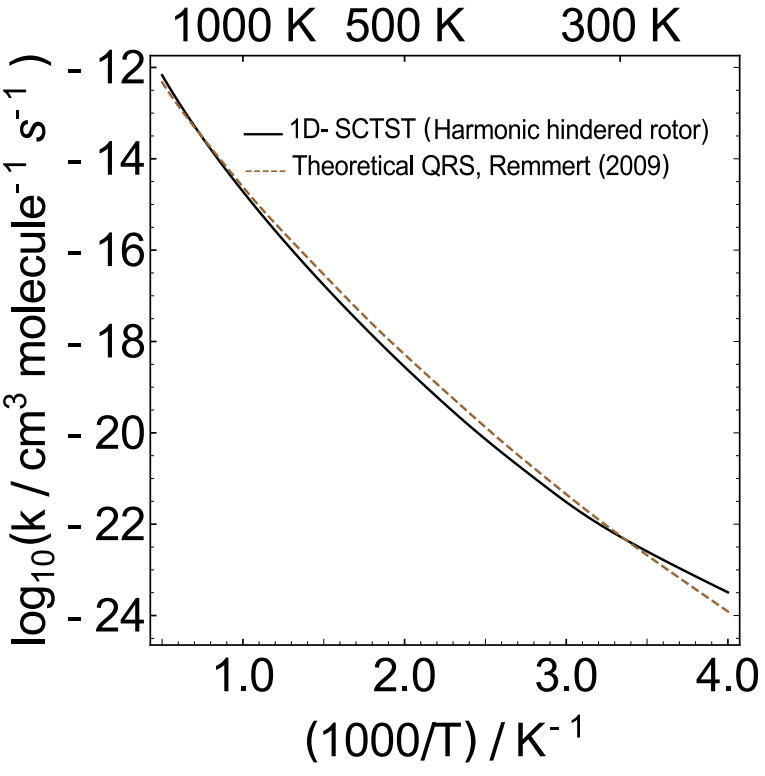

(b)

Figure 2: Arrhenius plots for the reaction $CH_3 + CH_4 \longrightarrow CH_4 + CH_3$. In (a) the results of SCTST calculations using the numerical solution to the hindered rotor partition function are compared to experiment[21, 22] and 2D-QRS calculations[24]. In (b), 1D-SCTST (this work) and 2D-QRS[24] are compared directly when the same treatment of the hindered rotor degree of freedom is used.

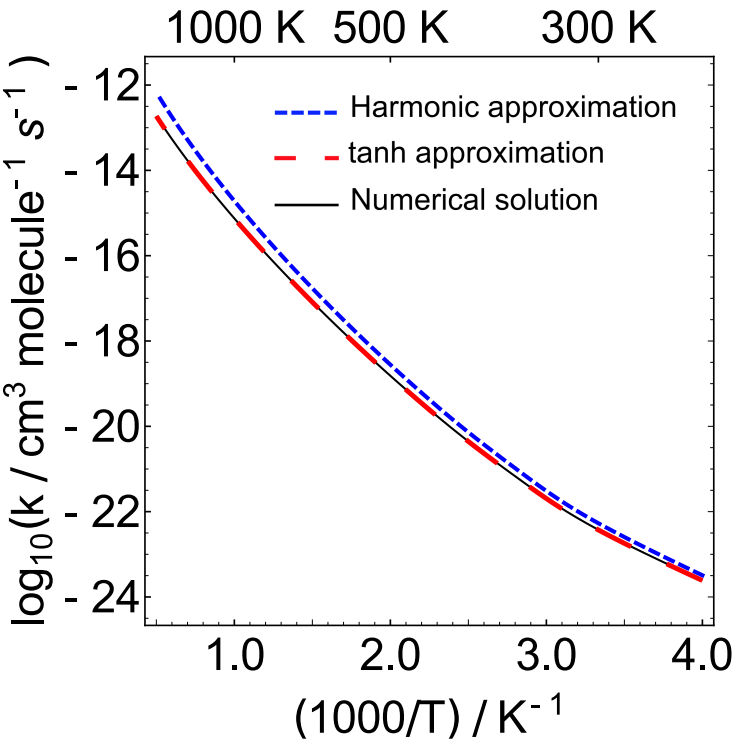

(a)

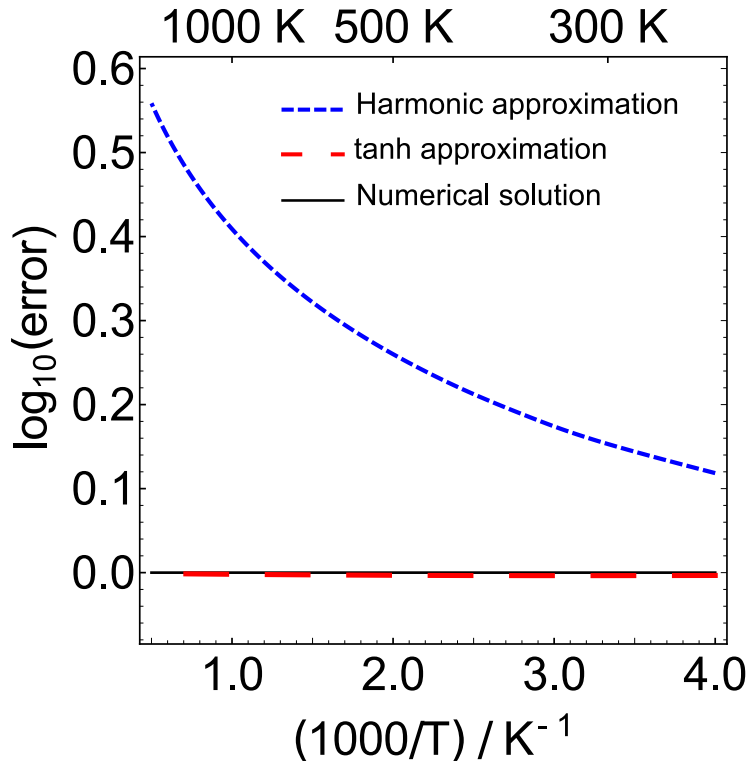

(b)

Figure 3: Rate constant comparisons for the reaction $CH_3 + CH_4 \longrightarrow CH_4 + CH_3$ using three treatments of the hindered rotor. In (a), the rates given by SCTST using three methods are shown in an Arrhenius plot. In (b) the results are compared by normalising by the numerical solution.

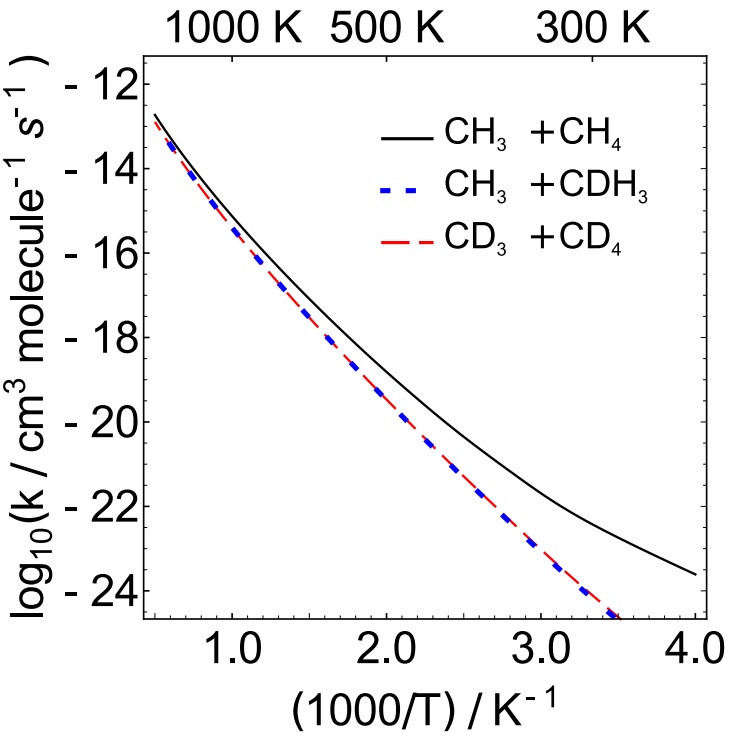

Figure 4: Thermal rate constant comparison for the $CH_3 + CH_4$ (R1) reaction and deuterium-substituted reactions $CH_3 + CH_3D$ (R2) and $CD_3 + CD_4$ (R3).

T(K)	$4k_2/k1$	k_3/k_1
300	0.0175 (0.056)	0.021 (0.020)
350	0.0548 (0.085)	0.062 (0.040)
400	0.106 (0.120)	0.116 (0.066)
450	0.162 (0.160)	0.170 (0.097)
500	0.215 (0.202)	0.222 (0.130)
550	0.264 (0.245)	0.270 (0.164)
600	0.308 (0.286)	0.311 (0.198)
800	0.445 (0.438)	0.440 (0.326)
1000	0.533 (0.564)	0.525 (0.433)
1500	0.646 (0.772)	0.635 (0.610)
2000	0.694 (0.870)	0.683 (0.698)

Table 4: Kinetic isotope effects in reactions R2 and R3. Values in brackets are those calculated from quantum reactive scattering calculations[24].

atoms with deuterium atoms. The secondary effect is much smaller, and in our calculations can increase or decrease the rate depending on temperature. These results are in good agreement with those of Remmert *et al.*[24] as shown in Table 4. The agreement with previous work is excellent for the primary effect ($4k_2/k1$) over

the whole temperature range. For the secondary effect, the agreement is worse for mid-range temperatures, between 400-600 K. This is likely a result of the improved treatment of the hindered rotor in this study; as R1 and R2 have the same HR frequency, their HR contributions will exactly cancel in the ratio $4k_2/k1$ and thus this ratio is insensitive to the hindered rotor treatment. R1 and R3, however, have differing hindered rotor frequencies, and so the ratio k_3/k_1 is dependent on the HR treatment.

5. Conclusions

One-dimensional semiclassical transition state theory (1D-SCTST) presents a computationally cheap way to include quantum tunneling effect in the calculation of chemical reaction rate constants. These calculations required only 11 *ab initio* calculations, of which 8 were calculated at the MP2 level of theory and 3 at the CCSD(T) level of theory; thus this is an inexpensive method that has scope to be used on much larger systems. We have shown it can produce results in good agreement with both experimental and quantum scattering results for the title reaction, and its isotopic analogues.

We have shown that the choice of treatment of the hindered rotor degree of freedom can significantly influence the results. Using a harmonic oscillator partition function overestimates the rate by about 200% at 500 K and over 300 % at 1500 K. The accuracy of the analytical tanh approximate hindered rotor partition function [32] has been tested by comparing its results to that of numerically solving the Schrödinger equation. We found that for this particular set of reactions, the tanh approximation, despite being considerably cheaper, is in an excellent agreement to the numerical results.

Acknowledgments

X. Shan and D. C. Clary acknowledge financial support from the Leverhulme Trust (Project Grant No. RPG-2013-321). T. A. H. Burd is grateful for support from the EPSRC Centre for Doctoral Training in Theory and Modelling in Chemical Sciences (Project Grant No. EP/L015722/1).

References

[1] G. Nyman, D. C. Clary, Quantum scattering calculations on the $CH_4 + OH \rightarrow CH_3 + H_2O$ reaction, Journal of Chemical Physics 101 (7) (1994) 5756–5771. doi:10.1063/1.467360.

[2] D. H. Zhang, H. Guo, Recent advances in quantum dynamics of bimolecular reactions, Annual Review of Physical Chemistry 67 (2016) 135–158.

[3] D. H. Zhang, H. Guo, Recent Advances in Quantum Dynamics of Bimolecular Reactions, Annual Review of Physical Chemistry 67 (1) (2016) 135–158. doi:10.1146/annurev-physchem-040215-112016.

[4] I. R. Craig, D. E. Manolopoulos, Quantum statistics and classical mechanics: Real time correlation functions from ring polymer molecular dynamics, Journal of Chemical Physics 121 (8) (2004) 3368–3373.

[5] I. R. Craig, D. E. Manolopoulos, Chemical reaction rates from ring polymer molecular dynamics, Journal of Chemical Physics 122 (8) (2005) 084106.

[6] S. Habershon, D. E. Manolopoulos, T. E. Markland, T. F. Miller III, Ring-polymer molecular dynamics: quantum effects in chemical dynamics from classical trajectories in an extended phase space, Annual Review of Physical Chemistry 64 (2013) 387–413.

[7] D. G. Truhlar, B. C. Garrett, Variational transition state theory, Annual Review of Physical Chemistry 35 (1) (1984) 159–189.

[8] J. Pu, D. G. Truhlar, Validation of variational transition state theory with multidimensional tunneling contributions against accurate quantum mechanical dynamics for $H + CH_4 \rightarrow H_2 + CH_3$ in an extended temperature interval, Journal of Chemical Physics 117 (4) (2002) 1479–1481.

[9] W. H. Miller, Semiclassical limit of quantum mechanical transition state theory for nonseparable systems, Journal of Chemical Physics 62 (5) (1975) 1899–1906. doi:10.1063/1.430676.

[10] W. H. Miller, Semi-classical theory for non-separable systems:. Construction of good action-angle variables for reaction rate constants, Faraday Discussions of the Chemical Society 62 (0) (1977) 40–46. doi:10.1039/DC9776200040.

[11] W. H. Miller, R. Hernandez, N. C. Handy, D. Jayatilaka, A. Willetts, Ab initio calculation of anharmonic constants for a transition state, with application to semiclassical transition state tunneling probabilities, Chemical Physics Letters 172 (1) (1990) 62–68. doi:10.1016/0009-2614(90)87217-F.

[12] A. F. Wagner, Improved Multidimensional Semiclassical Tunneling Theory, Journal of Physical Chemistry A 117 (49) (2013) 13089–13100. doi:10.1021/jp409720s.

[13] T. L. Nguyen, J. F. Stanton, J. R. Barker, A practical implementation of semi-classical transition state theory for polyatomics, Chemical Physics Letters 499 (1-3) (2010) 9–15. doi:10.1016/j.cplett.2010.09.015.

[14] C. Aieta, F. Gabas, M. Ceotto, An efficient computational approach for the calculation of the vibrational density of states, Journal of Physical Chemistry A 120 (27) (2016) 4853–4862.

[15] S. M. Greene, X. Shan, D. C. Clary, An investigation of one- versus two-dimensional semiclassical transition state theory for H atom abstraction and exchange reactions, Journal of Chemical Physics 144 (8) (2016) 084113. doi:10.1063/1.4942161.

[16] S. M. Greene, X. Shan, D. C. Clary, Reduced-dimensionality semiclassical transition state theory: Application to hydrogen atom abstraction and exchange reactions of hydrocarbons, Journal of Physical Chemistry A 119 (50) (2015) 12015–12027. doi:10.1021/acs.jpca.5b04379.

[17] S. M. Greene, X. Shan, D. C. Clary, Rate constants of chemical reactions from semiclassical transition state theory in full and one dimension, Journal of Chemical Physics 144 (24) (2016) 244116. doi:10.1063/1.4954840.

[18] X. Shan, J. C. Vincent, S. Kirkpatrick, M. D. Walker, M. R. Sambrook, D. C. Clary, A Combined Theoretical and Experimental Study of Sarin (GB) Decomposition at High Temperatures, Journal of Physical Chemistry Adoi:10.1021/acs.jpca.7b04282.

[19] M. H. Back, R. A. Back, Thermal decomposition and reactions of methane, Academic Press, New York, 1983.

[20] N. Kungwan, T. N. Truong, Kinetics of the hydrogen abstraction $CH_3 + \text{Alkane} \rightarrow CH_4 + \text{Alkyl}$ reaction class: An application of the reaction class transition state theory, Journal of Physical Chemistry A 109 (34) (2005) 7742–7750.

[21] F. Dainton, K. Ivin, F. Wilkinson, The kinetics of the exchange reaction $CH_3 + CH_4 \rightarrow CH_4 + CH_3$ using ^{14}C as a tracer, Transactions of the Faraday Society 55 (1959) 929–936.

[22] J. Kerr, M. Parsonage, Evaluated Kinetic Data on Gas Phase Hydrogen Transfer Reactions of Methyl Radicals, UMI, 1976.

[23] F. O. Rice, R. E. Varnerin, Activation energies of reactions of methyl radicals with organic molecules, Journal of the American Chemical Society 77 (1) (1955) 221–224.

[24] S. M. Remmert, S. T. Banks, D. C. Clary, Reduced Dimensionality Quantum Dynamics of $CH_3 + CH_4 \rightarrow CH_4 + CH_3$: Symmetric Hydrogen Exchange on an Ab Initio Potential, Journal of Physical Chemistry A 113 (16) (2009) 4255–4264. doi:10.1021/jp810803k.

[25] S. Ramazani, Direct-dynamics VTST study of hydrogen or deuterium abstraction and $C-C$ bond formation or dissociation in the reactions of $CH_3 + CH_4$, $CH_3 + CD_4$, $CH_3D + CD_3$, $CH_3CH_3 + H$, and $CH_3CD_3 + D$, Journal of Chemical Physics 138 (19) (2013) 194305.

[26] L. K. Huynh, A. Ratkiewicz, T. N. Truong, Kinetics of the hydrogen abstraction $OH + \text{Alkane} \rightarrow H_2O + \text{Alkyl}$ reaction class: An application of the reaction class transition state theory, Journal of Physical Chemistry A 110 (2) (2006) 473–484.

[27] B. Temelso, C. D. Sherrill, R. C. Merkle, R. A. Freitas, High-level ab initio studies of hydrogen abstraction from prototype hydrocarbon systems, Journal of Physical Chemistry A 110 (38) (2006) 11160–11173.

[28] A. Dybala-Defratyka, P. Paneth, J. Pu, D. G. Truhlar, Benchmark results for hydrogen atom transfer between carbon centers and validation of electronic structure methods for bond energies and barrier heights, Journal of Physical Chemistry A 108 (13) (2004) 2475–2486.

[29] M. Saeys, M.-F. Reyniers, G. B. Marin, V. Van Speybroeck, M. Waroquier, Ab initio calculations for hydrocarbons: enthalpy of formation, transition state geometry, and activation energy for radical reactions, Journal of Physical Chemistry A 107 (43) (2003) 9147–9159.

[30] M. L. Coote, M. A. Collins, L. Radom, Calculation of accurate imaginary frequencies and tunnelling coefficients for hydrogen abstraction reactions using ircmax, Molecular Physics 101 (9) (2003) 1329–1338.

[31] B. A. Ellingson, V. A. Lynch, S. L. Mielke, D. G. Truhlar, Statistical thermodynamics of bond torsional modes: Tests of separable, almost-separable, and improved pitzer–gwinn approximations, Journal of Chemical Physics 125 (8) (2006) 084305.

[32] Y.-Y. Chuang, D. G. Truhlar, Statistical thermodynamics of bond torsional modes, Journal of Chemical Physics (112) (2000) 1221. doi:10.1063/1.480768.

[33] S. M. Greene, X. Shan, D. C. Clary, Rate constants of chemical reactions from semiclassical transition state theory in full and one dimension, Journal of Chemical Physics 144 (24) (2016) 244116. doi:10.1063/1.4954840.

[34] V. Barone, Anharmonic vibrational properties by a fully automated second-order perturbative approach, Journal of Chemical Physics 122 (1) (2005) 014108. doi:10.1063/1.1824881.

[35] J. F. Stanton, Semiclassical Transition-State Theory Based on Fourth-Order Vibrational Perturbation Theory: The Symmetrical Eckart Barrier, Journal of Physical Chemistry Letters 7 (14) (2016) 2708–2713. doi:10.1021/acs.jpclett.6b01239.

[36] D. G. Truhlar, B. C. Garrett, S. J. Klippenstein, Current Status of Transition-State Theory, Journal of Physical Chemistry 100 (31) (1996) 12771–12800. doi:10.1021/jp953748q.

[37] J. Zheng, T. Yu, E. Papajak, I. M. Alecu, S. L. Mielke, D. G. Truhlar, Practical methods for including torsional anharmonicity in thermochemical calculations on complex molecules: The internal-coordinate multi-structural approximation, Physical Chemistry Chemical Physics 13 (23) (2011) 10885. doi:10.1039/c0cp02644a.

[38] Ching Yeh Lin, E. I. Izgorodina, M. L. Coote, How accurate are approximate methods for evaluating partition functions for hindered internal rotations?, Journal of Chemical Physics A 112 (9) (2008) 1956–1964. doi:10.1021/JP710341H.

[39] K. S. Pitzer, W. D. Gwinn, Energy Levels and Thermodynamic Functions for Molecules with Internal Rotation I. Rigid Frame with Attached Tops, Journal of Chemical Physics 10 (7) (1942) 428–440. doi:10.1063/1.1723744.

[40] T. H. Dunning Jr, Gaussian basis sets for use in correlated molecular calculations. i. the atoms boron through neon and hydrogen, Journal of Chemical Physics 90 (2) (1989) 1007–1023.

[41] M. J. Frisch, G. W. Trucks, H. B. Schlegel, G. E. Scuseria, M. A. Robb, J. R. Cheeseman, G. Scalmani, V. Barone, B. Mennucci, G. A. Petersson, H. Nakatsuji, M. Caricato, X. Li, H. P. Hratchian, A. F. Izmaylov, J. Bloino, G. Zheng, J. L. Sonnenberg, M. Hada, M. Ehara, K. Toyota, R. Fukuda, J. Hasegawa, M. Ishida, T. Nakajima, Y. Honda, O. Kitao, H. Nakai, T. Vreven, J. A. Montgomery, Jr., J. E. Peralta, F. Ogliaro, M. Bearpark, J. J. Heyd, E. Brothers, K. N. Kudin, V. N. Staroverov, R. Kobayashi, J. Normand, K. Raghavachari, A. Rendell, J. C. Burant, S. S. Iyengar, J. Tomasi, M. Cossi, N. Rega, J. M. Millam, M. Klene, J. E. Knox, J. B. Cross, V. Bakken, C. Adamo, J. Jaramillo, R. Gomperts, R. E. Stratmann, O. Yazyev, A. J. Austin, R. Cammi, C. Pomelli, J. W. Ochterski, R. L. Martin, K. Morokuma, V. G. Zakrzewski, G. A. Voth, P. Salvador, J. J. Dannenberg, S. Dapprich, A. D. Daniels, . Farkas, J. B. Foresman, J. V. Ortiz, J. Cioslowski, D. J. Fox, Gaussian09 Revision E.01, gaussian Inc. Wallingford CT 2009.

[42] D. G. Truhlar, Basis-set extrapolation, Chemical Physics Letters 294 (1) (1998) 45–48.

[43] A. Fernandez-Ramos, D. G. Truhlar, Improved algorithm for corner-cutting tunneling calculations, Journal of Chemical Physics 114 (4) (2001) 1491–1496.

[44] T. L. Nguyen, J. F. Stanton, High-level theoretical study of the reaction between hydroxyl and ammonia: Accurate rate constants from 200 to 2500 K, Journal of Chemical Physics 147 (15) (2017) 152704.

6. Supporting Information

Rate constants in the temperature range 250 K - 2000 K for R1 (TST, Harmonic, tanh, numerical), R2(numerical) and R3 (numerical) are tabulated in table below. Powers of ten are in parentheses.

T(K)	k1(TST)	k1(Numerical)	k1(tanh)	k1(Harmonic)	k2(Numerical)	k3(Numerical)
250.0	6.89575084692(-28)	1.62388936509(-24)	1.59669680636(-24)	2.43883515765(-24)	9.3356784206(-28)	5.01397055821(-27)
300.0	2.33142342552(-25)	3.04095190901(-23)	2.99187561233(-23)	4.87328378812(-23)	1.28688138395(-25)	6.3641974782(-25)
350.0	1.53050789551(-23)	4.17544554546(-22)	4.11178183612(-22)	7.09176119896(-22)	5.54498136541(-24)	2.57419856614(-23)
400.0	3.62172163239(-22)	4.01446090628(-21)	3.9570338865(-21)	7.1854113638(-21)	1.04361982051(-22)	4.63464653736(-22)
450.0	4.34843569934(-21)	2.75400123781(-20)	2.71707862011(-20)	5.17003983799(-20)	1.0944813305(-21)	4.71219406233(-21)
500.0	3.24878591809(-20)	1.41702423265(-19)	1.39920750682(-19)	2.77889468458(-19)	7.51721139502(-21)	3.16630159864(-20)
550.0	1.71884258055(-19)	5.76474766182(-19)	5.69663895149(-19)	1.17694756833(-18)	3.76763572444(-20)	1.56214387148(-19)
600.0	7.01741842523(-19)	1.93992647255(-18)	1.9183369671(-18)	4.11120315811(-18)	1.48438322269(-19)	6.08420079281(-19)
650.0	2.34581006787(-18)	5.59813227775(-18)	5.53929562818(-18)	1.22836539673(-17)	4.84541296694(-19)	1.96920320094(-18)
700.0	6.69785200115(-18)	1.42488313648(-17)	1.41070681543(-17)	3.22996237278(-17)	1.36146065409(-18)	5.49790100565(-18)
750.0	1.68480196207(-17)	3.26982321465(-17)	3.23895404306(-17)	7.64228755189(-17)	3.38760926206(-18)	1.36141329796(-17)
800.0	3.82129965874(-17)	6.88258343509(-17)	6.82078020901(-17)	1.65566980564(-16)	7.62688414998(-18)	3.05383070417(-17)
850.0	7.95480887143(-17)	1.34701567274(-16)	1.33548895685(-16)	3.32998694119(-16)	1.57976385021(-17)	6.30756205302(-17)
900.0	1.54102169569(-16)	2.47809113974(-16)	2.45783872827(-16)	6.28674926211(-16)	3.05005257092(-17)	1.21513935091(-16)
950.0	2.80862455508(-16)	4.3231851004(-16)	4.28938163908(-16)	1.12409470861(-15)	5.54646394712(-17)	2.20595062664(-16)
1000.0	4.85837268117(-16)	7.20360058036(-16)	7.14962118591(-16)	1.91752391503(-15)	9.58014075758(-17)	3.8051766382(-16)
1050.0	8.03324044153(-16)	1.15325065976(-15)	1.1449548822(-15)	3.13944195962(-15)	1.58255408271(-16)	6.27926079803(-16)
1100.0	1.27711466821(-15)	1.7826299706(-15)	1.77030273587(-15)	4.95806331303(-15)	2.5144223506(-16)	9.96855418141(-16)
1150.0	1.96161031949(-15)	2.67148919294(-15)	2.65370213188(-15)	7.58479900139(-15)	3.86067578027(-16)	1.5295953337(-15)
1200.0	2.92279963428(-15)	3.89504501112(-15)	3.87004677962(-15)	1.12795410447(-14)	5.75118190558(-16)	2.27744878633(-15)
1250.0	4.23911486757(-15)	5.54149190153(-15)	5.50716654219(-15)	1.63556733228(-14)	8.340275324(-16)	3.30138902476(-15)
1300.0	6.00212075396(-15)	7.71257858108(-15)	7.66641317074(-15)	2.31847335299(-14)	1.18080719357(-15)	4.67257490149(-15)
1350.0	8.31704649896(-15)	1.05240293722(-14)	1.04630938543(-14)	3.2200671219(-14)	1.63614627479(-15)	6.4727585491(-15)
1400.0	1.13031752099(-14)	1.4105830643(-14)	1.40267581843(-14)	4.39036654804(-14)	2.22348172834(-15)	8.79454783971(-15)
1450.0	1.5094134196(-14)	1.860243509(-14)	1.85013475202(-14)	5.88634820284(-14)	2.96904843283(-15)	1.17416151638(-14)
1500.0	1.98379032627(-14)	2.41726559449(-14)	2.40452180401(-14)	7.77223631581(-14)	3.90187327605(-15)	1.54286833157(-14)
1550.0	2.56968920069(-14)	3.09896870819(-14)	3.08310501513(-14)	1.01197455199(-13)	5.05378253694(-15)	1.99815222892(-14)
1600.0	3.28477783265(-14)	3.92408610954(-14)	3.90456575798(-14)	1.30082786868(-13)	6.4593622473(-15)	2.55368386261(-14)
1650.0	4.14812699634(-14)	4.9127346128(-14)	4.88897095414(-14)	1.65250818554(-13)	8.1559035664(-15)	3.22420643058(-14)
1700.0	5.18018501277(-14)	6.08638483581(-14)	6.05773790377(-14)	2.0765358733(-13)	1.01833453382(-14)	4.02549997911(-14)
1750.0	6.40274403211(-14)	7.46782351754(-14)	7.43359296674(-14)	2.58323475634(-13)	1.2584200805(-14)	4.97437197667(-14)

1800.0	7.83887802633(-14)	9.08108461796(-14)	9.0405252481(-14)	3.1837363343(-13)	1.540342926(-14)	6.08859301296(-14)
1850.0	9.51293587937(-14)	1.09514461368(-13)	1.09037363421(-13)	3.88998084412(-13)	1.86884165992(-14)	7.38687784412(-14)
1900.0	1.14504167325(-13)	1.31052915688(-13)	1.30495870848(-13)	4.71471546783(-13)	2.24887251516(-14)	8.88883351399(-14)
1950.0	1.36779862855(-13)	1.55701356825(-13)	1.55055421597(-13)	5.67148998433(-13)	2.68561211634(-14)	1.06149225212(-13)
2000.0	1.62234292634(-13)	1.83745759745(-13)	1.83001132972(-13)	6.77465015155(-13)	3.18444774199(-14)	1.25864212603(-13)